

Evolution of phases and microstructure in $\text{Fe}_{81}\text{B}_{13.5}\text{Si}_{3.5}\text{C}_2$ metallic glass during electron-beam and pulsed-laser irradiation

M. Sorescu and E. T. Knobbe

Oklahoma State University, Department of Chemistry, Stillwater, Oklahoma 74078-0447

D. Barb

Institute of Atomic Physics, P.O. Box MG/7, R 76900 Bucharest-Magurele, Romania

(Received 12 August 1994)

A comparative study of electron-beam and pulsed-laser irradiation effects in metallic glasses has been performed in order to understand the relationship between magnetic behavior and select variations in the structural characteristics of alloy phases. Samples of $\text{Fe}_{81}\text{B}_{13.5}\text{Si}_{3.5}\text{C}_2$ metallic glass were irradiated with a pulsed excimer laser ($\lambda=308$ nm, $\tau=10$ ns), with a high-energy electron beam ($W=7$ MeV), and with low-energy electron beams ($W=30$ and 50 keV). Irradiation-driven changes in the magnetic anisotropy and phase equilibrium of alloy samples were studied by Mössbauer spectroscopy and scanning electron microscopy. Complementary information was obtained using energy-dispersive x-ray analysis. High-energy electron-beam irradiation was found to induce an out-of-plane magnetic anisotropy due to changes in the chemical short-range order. Low-energy electron-beam irradiation resulted in the formation of crystalline regions, in which α -Fe, Fe-Si, Fe_3B , Fe_2B , and clusters of γ -Fe were identified. Interpretation of these results is given in terms of radiation-enhanced diffusion. Pulsed-excimer-laser irradiation was found to induce controlled magnetic anisotropy without onset of bulk crystallization in the $\text{Fe}_{81}\text{B}_{13.5}\text{Si}_{3.5}\text{C}_2$ amorphous system. The effect of excimer-laser-induced amorphization was evidenced in thermally annealed $\text{Fe}_{81}\text{B}_{13.5}\text{Si}_{3.5}\text{C}_2$ samples and explained using melt model calculations. In all cases studied, the key to explaining the irradiation-induced property modifications is the underlying alloy microstructure.

I. INTRODUCTION

Recent investigations of irradiation-induced effects in metallic glasses have been performed with regard to the potential use of amorphous alloys as radiation-resistant materials. Neutron and ion-beam irradiation studies have shown that structural modifications in radiation-exposed alloys determine changes in their soft magnetic properties.¹⁻³ Cw laser irradiation has been found to promote structural relaxation and/or crystallization in amorphous ferromagnetic ribbons.^{4,5} Different stress distributions have been obtained in metallic glasses, as a result of inhomogeneous heat flows produced by local laser annealing.^{6,7} Improved thermal stability and modified crystallization kinetics have been observed after picosecond laser treatment in several binary amorphous alloys.⁸ Pulsed-excimer-laser irradiation has been suggested as an intriguing means of controlling the magnetic anisotropy and phase equilibrium in amorphous and nanocrystalline materials.⁹⁻¹⁴ Similarly, electron-beam irradiation has been used as a means of accelerating diffusion in Fe-Ni alloys.¹⁵

In order to understand the relationship between magnetic parameters and structural characteristics of alloy phases, a promising approach is to address the phase evolution and microstructure development during various irradiation treatments. The present study was carried out in order to investigate the effect of electron-beam irradiation on the magnetic and structural properties of

$\text{Fe}_{81}\text{B}_{13.5}\text{Si}_{3.5}\text{C}_2$ amorphous alloy and compare it with the effect of pulsed-excimer-laser irradiation of the same amorphous material. Because of its local-probe character, Mössbauer spectroscopy was used to monitor the changes in magnetic anisotropy and phase composition, induced by employing different values of the irradiation parameters in both treatments performed. Related morphological changes were examined by scanning electron microscopy (SEM), and the resultant crystalline precipitates were characterized by energy-dispersive x-ray analysis (EDX). Irradiation-driven property changes are discussed in terms of phenomenological models in which the underlying alloy microstructure played an essential role.

II. EXPERIMENTAL PROCEDURES

A. Irradiation treatments

Amorphous alloy $\text{Fe}_{81}\text{B}_{13.5}\text{Si}_{3.5}\text{C}_2$ (Metglas 2605 SC) was supplied by Allied Signal Inc. in the form of $20\text{-}\mu\text{m}$ -thick ribbons. The material has a crystallization temperature of 480°C and a magnetostriction constant¹⁶ of 30×10^{-6} . Square samples (2×2 cm) were cut from the foils and exposed on the shiny side to the $\lambda=308\text{-nm}$ radiation generated by a XeCl excimer laser (Lambda Physik), with the pulse width $\tau=10$ ns, capable of giving an energy $W_p=75$ mJ/pulse. A single-pulse energy density of 3 J/cm^2 , corresponding to a laser fluence $\Phi_L=5 \times 10^{18}$

photons/cm² was achieved by focusing with a cylindrical fused-silica lens to a spot size of 0.5×5 mm². Amorphous samples of $\text{Fe}_{81}\text{B}_{13.5}\text{Si}_{3.5}\text{C}_2$ were irradiated with 2, 5, and 10 laser pulses per spot at a repetition rate of 1 Hz. An acceptable degree of homogeneity was obtained by laser-beam scanning of the sample surface, which was placed on an x - y - z micrometer translation stage.

Thermally treated $\text{Fe}_{81}\text{B}_{13.5}\text{Si}_{3.5}\text{C}_2$ samples were prepared by annealing the amorphous specimens at 375 and 450 °C for 1 h. These samples were further exposed to pulsed-excimer-laser irradiation ($\lambda = 308$ nm, $\tau = 10$ ns, $\Phi_L = 5 \times 10^{18}$ photons/cm², $N = 2$ laser pulses/spot, repetition rate 1 Hz). All laser treatments were performed in air at room temperature.

A different set of amorphous $\text{Fe}_{81}\text{B}_{13.5}\text{Si}_{3.5}\text{C}_2$ samples were packed in aluminum foils and exposed to high-energy electron-beam irradiation. The electrons had an energy $W = 7$ MeV and electron fluences of 4.1×10^{14} and 1.3×10^{15} electrons/cm² were employed.

Finally, a series of $\text{Fe}_{81}\text{B}_{13.5}\text{Si}_{3.5}\text{C}_2$ amorphous specimens were subjected to irradiation with low energy electrons ($W = 30$ and 50 keV). The samples were fixed in a metallic frame and mounted to a rotating cylinder. The minimum intensity of the electron current was 1 mA, so that a fluence $\Phi_E = 2.4 \times 10^{15}$ electrons/cm² was obtained.

B. Experimental techniques

Room-temperature transmission Mössbauer spectra were recorded with the γ ray perpendicular to the ribbon plane using a constant acceleration spectrometer (Ranger Scientific). The 25-mCi γ -ray source was ⁵⁷Co diffused in Rh matrix. Least-squares fitting of the Mössbauer spectra corresponding to the amorphous, annealed, and irradiated samples was performed with the NORMOS DIST program¹⁷ in the assumption of Lorentzian line shapes. The program uses the constrained Hesse-Rübartsch method to extract the hyperfine field distributions and can analyze superpositions of field distributions and crys-

talline sites. The relative areas of the outer:inner line pairs of the amorphous component were constrained to the ratio 3:1. The relative intensities of lines one, two and three for each pattern were correlated to be the same for all crystalline subspectra.

SEM investigations were performed without further surface preparation with a JEOL electron microscope at 25 keV, operating in the secondary-electron-emission mode. Chemical analysis of select microvolumes in the partially crystallized and irradiated samples was carried out with a Tracor Northern EDX spectrometer. The technique employed was sensitive to chemical elements $Z > 11$ and provided an average chemical composition over a volume of a cubic micron.¹⁸

III. RESULTS AND DISCUSSION

A. High-energy electron-beam irradiation effects in $\text{Fe}_{81}\text{B}_{13.5}\text{Si}_{3.5}\text{C}_2$ metallic glass

Room-temperature transmission Mössbauer spectra of the $\text{Fe}_{81}\text{B}_{13.5}\text{Si}_{3.5}\text{C}_2$ samples, exposed to high-energy electron-beam irradiation ($W = 7$ MeV) at fluences of 4.1×10^{14} and 1.3×10^{15} electrons/cm², are shown in Figs. 1(a) and 1(b), respectively. The broad absorption lines in the Mössbauer spectra are due to the various nearest-neighbor configurations of the resonant atoms in the amorphous structure. The different inequivalent sites determine fluctuations of the hyperfine parameters, which are described in terms of the corresponding distributions. Figures 1(A) and 1(B) show the hyperfine magnetic-field distributions extracted from the Mössbauer spectra of the irradiated $\text{Fe}_{81}\text{B}_{13.5}\text{Si}_{3.5}\text{C}_2$ samples. The refined values of the hyperfine parameters corresponding to the as-quenched and high-energy electron-irradiated $\text{Fe}_{81}\text{B}_{13.5}\text{Si}_{3.5}\text{C}_2$ system are listed in Table I.

For the 14.4-keV γ rays of ⁵⁷Fe, the relative intensity of the second (fifth) to the first (sixth) lines is given in the thin absorber approximation, by (Ref. 19) $R_{21} = 4 \sin^2 \alpha / [3(1 + \cos^2 \alpha)]$, where α is the angle between the γ -ray

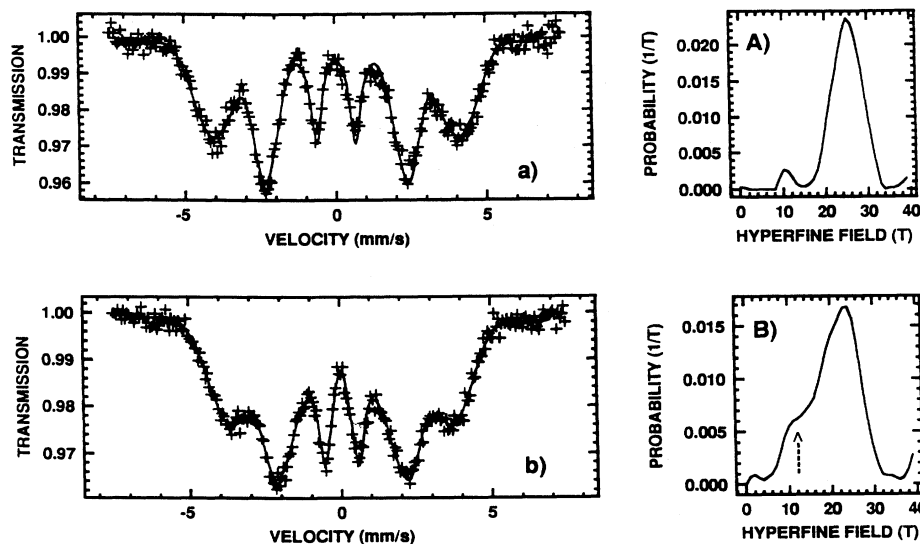


FIG. 1. Room-temperature transmission Mössbauer spectra of the $\text{Fe}_{81}\text{B}_{13.5}\text{Si}_{3.5}\text{C}_2$ samples, after high-energy electron-beam irradiation: (a) $W = 7$ MeV, $\Phi_E = 4.1 \times 10^{14}$ electrons/cm²; (b) $W = 7$ MeV, $\Phi_E = 1.3 \times 10^{15}$ electrons/cm². Velocity scale is calibrated relative to α -Fe at 300 K. The hyperfine magnetic-field distributions extracted from these spectra are shown in (A) and (B). The marker indicates the low-field component of the hyperfine magnetic-field distribution.

TABLE I. Relative intensity of lines R_{21} , average hyperfine magnetic field $\langle H_{\text{hf}} \rangle$, mean hyperfine field $(H_{\text{hf}})_m$, width of the hyperfine magnetic-field distribution ΔH_{hf} , and total absorption area in the Mössbauer spectra of the $\text{Fe}_{81}\text{B}_{13.5}\text{Si}_{3.5}\text{C}_2$ system, as a function of the electron fluence Φ_E employed in high-energy electron-beam irradiation.

Φ_E (electrons/cm ²)	R_{21}	$\langle H_{\text{hf}} \rangle$ (kOe)	$(H_{\text{hf}})_m$ (kOe)	ΔH_{hf} (kOe)	Resonant area (a.u.)
0	1.11	251.1	255.2	45.5	0.219
4.1×10^{14}	0.93	245.9	250.1	48.1	0.221
1.3×10^{15}	0.74	205.5	212.2	66.3	0.238
Errors:	± 0.02	± 1.2	± 1.2	± 1.5	± 0.003

propagation direction and the direction of the net magnetic moment. The ratio R_{21} varies from 0 to $\frac{4}{3}$ as α changes from 0° to 90° and for a completely random distribution of magnetic-moment directions, takes the value 0.67. Consequently, the fluence-dependent decrease in the areal ratio R_{21} , inferred from Table I, indicates a gradual tendency of the average magnetic-moment direction to rotate out of the ribbon plane. Considering the threshold value $W_0 \sim 1$ MeV above which defects are formed in direct collisions,²⁰ we suggest that the decrease in the second and fifth Mössbauer line intensities of $\text{Fe}_{81}\text{B}_{13.5}\text{Si}_{3.5}\text{C}_2$ is due to defects induced by the high-energy electron irradiation, which are responsible for the reorientation of spins around the stress centers. Indeed, it has been shown that the formation of stresses induces an easy magnetization direction out of the sample plane through positive magnetostriction.^{1,9,21,22}

Further insight into the mechanism responsible for the electron-irradiation-induced magnetic anisotropy in $\text{Fe}_{81}\text{B}_{13.5}\text{Si}_{3.5}\text{C}_2$ is provided by the trends observed in the values of the average hyperfine magnetic field $\langle H_{\text{hf}} \rangle$ and the width of the hyperfine field distribution ΔH_{hf} . It can be seen by examination of Table I that the average value of the hyperfine magnetic field decreases gradually as a consequence of the high-energy electron irradiation, reflecting changes in the magnetic properties of the $\text{Fe}_{81}\text{B}_{13.5}\text{Si}_{3.5}\text{C}_2$ amorphous phase. Moreover, the observed increase in the width of the hyperfine field distribution ΔH_{hf} with increasing electron fluence (Table I) suggests the occurrence of radiation-induced structural changes, consisting of the formation of new environments of the resonant atoms. The presence of two distinct types of resonant atom surroundings [Figs. 1(A) and 1(B)] is clearly observed at the highest electron fluence employed. The high-field peak of the field distribution can be associated with Fe atoms having primarily Si atoms as nearest neighbors, whereas the low-field component can be assigned to Fe atoms surrounded mainly by B atoms.²² Indeed, atomic rearrangements leading to the precipitation of Fe-Si clusters were found to precede the onset of crystallization in several studies on the $\text{Fe}_{81}\text{B}_{13.5}\text{Si}_{3.5}\text{C}_2$ system.²²⁻²⁴ Due to the low solubility of B in the Fe-Si alloy structure,^{25,26} the presence of Si atoms at Fe sites limits the diffusion of B atoms, causing a significant in-

crease in the number of Fe atoms having mostly B atoms as nearest neighbors. This further explains the pronounced increase in the low-field component of the hyperfine magnetic field distribution [Fig. 1(B)], as well as the observed decrease in the average value of the hyperfine magnetic field with increasing electron fluence. For the $\text{Fe}_{81}\text{B}_{13.5}\text{Si}_{3.5}\text{C}_2$ sample irradiated at the highest electron fluence, one may also note that the total absorption area (proportional to the recoilless fraction f of the amorphous phase) increases by $\sim 8\%$ over that of the as-quenched sample (Table I). A similar increase in the total resonant area preceding the onset of crystallization was observed in $\text{Fe}_{81}\text{B}_{13.5}\text{Si}_{3.5}\text{C}_2$ samples subjected to isochronal annealing treatments.²²

The decrease in the average hyperfine magnetic field and increase in the width of the field distribution consequently support the occurrence of chemical changes in the short-range order of the $\text{Fe}_{81}\text{B}_{13.5}\text{Si}_{3.5}\text{C}_2$ system, as an effect of the high-energy electron-beam irradiation per-

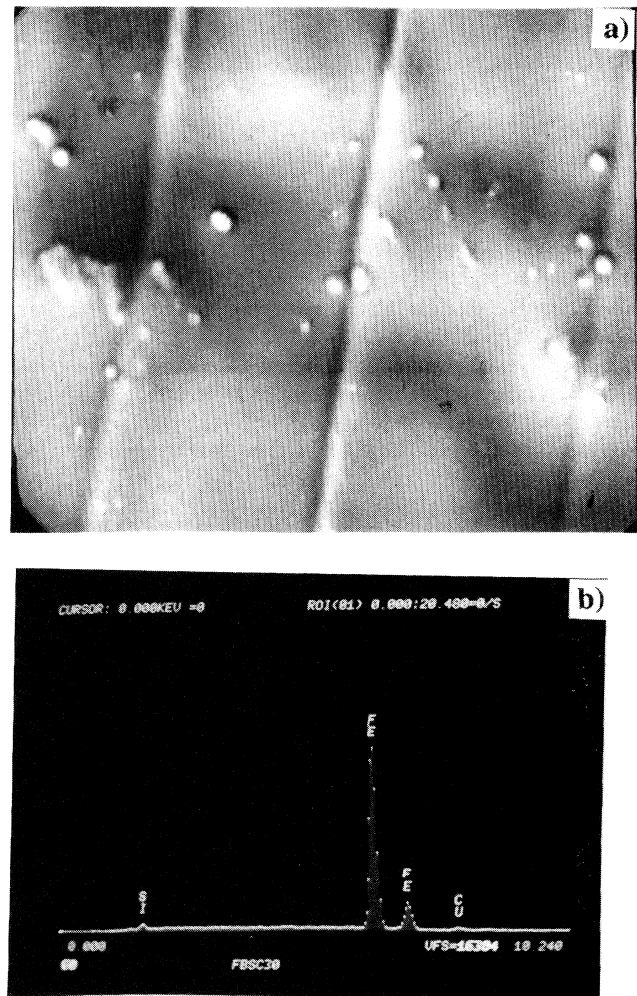


FIG. 2. (a) SEM photograph ($\times 1500$) and (b) EDX examination of the $\text{Fe}_{81}\text{B}_{13.5}\text{Si}_{3.5}\text{C}_2$ sample, after low-energy electron-beam irradiation ($W = 30$ keV, $\Phi_E = 2.4 \times 10^{15}$ electrons/cm²). Fe and Si peaks stand for the sample, whereas Cu impurities come from the tape.

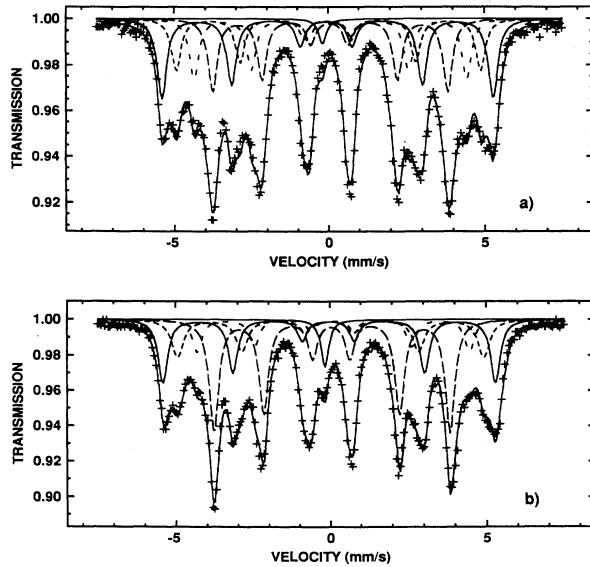


FIG. 3. Room-temperature transmission Mössbauer spectra of the $\text{Fe}_{81}\text{B}_{13.5}\text{Si}_{3.5}\text{C}_2$ samples, after low-energy electron-beam irradiation: (a) $W = 30$ keV, $\Phi_E = 2.4 \times 10^{15}$ electrons/cm²; (b) $W = 50$ keV, $\Phi_E = 2.4 \times 10^{15}$ electrons/cm².

formed. We suggest that the mechanism of irradiation-induced magnetic anisotropy, demonstrated by the fluence-dependent decrease in the magnetic texture parameter R_{21} , originates in the formation of stress centers which result from local atomic rearrangements in the irradiated $\text{Fe}_{81}\text{B}_{13.5}\text{Si}_{3.5}\text{C}_2$ amorphous system. Thus, the stress fields associated with the irradiation-induced microstructural defects are responsible for the reorientation of magnetic-moment directions in the metallic glass matrix.

B. Low-energy electron-beam irradiation effects in $\text{Fe}_{81}\text{B}_{13.5}\text{Si}_{3.5}\text{C}_2$ metallic glass

Figure 2(a) shows the SEM micrograph of the $\text{Fe}_{81}\text{B}_{13.5}\text{Si}_{3.5}\text{C}_2$ sample, after irradiation with low-energy electrons ($W = 30$ keV) at a fluence of 2.4×10^{15} electrons/cm². SEM examinations reveal the presence of micron-size crystalline islands in the electron-irradiated $\text{Fe}_{81}\text{B}_{13.5}\text{Si}_{3.5}\text{C}_2$ sample. Moreover, EDX analysis of select microvolumes [Fig. 2(b)] suggests the formation of Fe-Si precipitates on the irradiated surface. In order to gain additional information regarding the nature of the crystalline products and their dependence on electron-beam energy, Mössbauer spectroscopy measurements have also been performed, since they provide information on the dynamics of the magnetic texture and structural evolution of different crystalline phases.²⁷

Room-temperature transmission Mössbauer spectra of the $\text{Fe}_{81}\text{B}_{13.5}\text{Si}_{3.5}\text{C}_2$ samples, irradiated at a fluence of 2.4×10^{15} electrons/cm² with electron energies of 30 and 50 keV, are shown in Figs. 3(a) and 3(b), respectively. Table II presents the fitted values of the hyperfine parameters corresponding to the different phases formed in the low-energy electron-irradiated $\text{Fe}_{81}\text{B}_{13.5}\text{Si}_{3.5}\text{C}_2$ system. On the grounds of the values obtained for the room-temperature Mössbauer parameters, the first sextet in Table II can be assigned to α -Fe, an identification which is in agreement with results of isothermal and radiofrequency annealing studies on the $\text{Fe}_{81}\text{B}_{13.5}\text{Si}_{3.5}\text{C}_2$ system.^{28–33} The second six-line pattern can be attributed to a bcc Fe-Si alloy;^{22,28} the broadened absorption lines suggest the presence of Fe atoms with different numbers of Si nearest neighbors. Similarly, the third and fourth sextets can be assigned to Fe_3B and Fe_2B crystalline phases, respectively. As can be seen in Table II, the amount of stable Fe_2B phase in the $\text{Fe}_{81}\text{B}_{13.5}\text{Si}_{3.5}\text{C}_2$ specimen irradiated with 50-keV electrons is significantly

TABLE II. Hyperfine magnetic field H_{hf} , isomer shift δ (relative to α -Fe at 300 K), full width at half maxima w , intensity ratio R_{21} , and relative areas corresponding to the component patterns in the Mössbauer spectra of low-energy electron-beam irradiated $\text{Fe}_{81}\text{B}_{13.5}\text{Si}_{3.5}\text{C}_2$ samples.

W (keV)	Subspectrum No.	H_{hf} (kOe)	δ (mm/s)	w (mm/s)	R_{21}	Relative areas (%)	Assignment of sites
30	I	330.8	0.001	0.36	0.83	14.4	α -Fe
	II	304.2	0.050	0.44	0.83	9.9	Fe-Si
	III	272.7	0.106	0.36	0.83	11.4	Fe_3B
	IV	235.6	0.110	0.36	0.83	13.7	Fe_2B
	V		-0.090	0.30		1.1	γ -Fe
	VI	256.6	0.077		0.59	49.5	Amorphous
50	I	331.5	0.002	0.36	0.83	15.8	α -Fe
	II	305.5	0.060	0.44	0.83	10.9	Fe-Si
	III	272.1	0.105	0.36	0.83	7.6	Fe_3B
	IV	236.1	0.110	0.36	0.83	26.2	Fe_2B
	V		-0.088	0.30		2.5	γ -Fe
	VI	259.3	0.083		0.52	37.0	Amorphous
Errors:		± 1.5	± 0.015	± 0.02	± 0.02	± 1.0	

higher than in the sample subjected to bombardment with electrons having an energy of 30 keV. At the same time, the fraction of metastable Fe_3B phase formed in the $\text{Fe}_{81}\text{B}_{13.5}\text{Si}_{3.5}\text{C}_2$ sample irradiated at the electron energy of 50 keV is correspondingly lower than that produced in the sample exposed to 30-keV electrons. These results tend to support the reported formation of the equilibrium phase mixture $\alpha\text{-Fe} + \text{Fe}_2\text{B}$ at the point of impingement and of the three-phase mixture $\alpha\text{-Fe} + \text{Fe}_3\text{B} + \text{Fe}_2\text{B}$ in zones adjacent to the lased area in the high-fluence laser-beam irradiation study of $\text{Fe}_{80}\text{B}_{20}$ amorphous alloy.³⁴ The fifth subspectrum in Table II corresponds to a singlet exhibiting a negative chemical shift and has been assigned to $\gamma\text{-Fe}$ clusters. The isomer shift value is in excellent agreement with Mössbauer results on $\gamma\text{-Fe}$ precipitates in Cu,^{35,36} which were found to be paramagnetic at room temperature and present antiferromagnetic order below the Néel temperature $T_N \sim 70$ K. One may note that the formation of $\gamma\text{-Fe}$ clusters, not encountered in conventional thermal annealing studies of metallic glasses,²⁸⁻³¹ was reportedly observed in a Fe 2% Si alloy irradiated with subthreshold-energy electrons.³⁷ It can be inferred from Table II and Fig. 3 that the amount of $\gamma\text{-Fe}$ phase in the $\text{Fe}_{81}\text{B}_{13.5}\text{Si}_{3.5}\text{C}_2$ sample irradiated with 50-keV electrons is higher than in the specimen exposed to electrons having an energy of 30 keV. As indicated by the corresponding R_{21} values given in Table II, the crystalline phases formed in the irradiated alloy are strongly textured, suggesting the development of crystallization along preferred directions. Finally, the balance of the composition of the electron-irradiated $\text{Fe}_{81}\text{B}_{13.5}\text{Si}_{3.5}\text{C}_2$ samples is represented by an amorphous component, described by the respective field distribution. It presumably originates in the regions located at the edges of the irradiated zone, which experience a lower temperature during the electron-beam treatment. The rather high values of the average hyperfine magnetic field, however, suggest the occurrence of ordering processes in the amorphous matrix of the electron-irradiated $\text{Fe}_{81}\text{B}_{13.5}\text{Si}_{3.5}\text{C}_2$ samples.

The low-energy electron-beam irradiation effects observed in $\text{Fe}_{81}\text{B}_{13.5}\text{Si}_{3.5}\text{C}_2$ metallic glass in the present study can be understood in terms of radiation-enhanced diffusion.³⁸ The formation of stable regions with different crystalline structures is regarded as occurring in mass fluxes³⁷ maintained by the temperature gradient in the sample. A typical spatial formation of crystalline phases observed in the electron-irradiated $\text{Fe}_{81}\text{B}_{13.5}\text{Si}_{3.5}\text{C}_2$ metallic glass is shown in the SEM micrographs of Figs. 4(a) and 4(b). The out-of-plane geometry of the irradiated zone, as well as the observation that the foil thickness is decreased at the center and increased at the boundary of the irradiated region, support the occurrence of mass transfer in the electron-irradiated metallic alloy. Estimated temperatures³⁷ of 950–1000 °C at the center and 450–500 °C at the edges of the electron-exposed surfaces determine the formation of thermal gradients, which drive the mass fluxes in the irradiated material.

The present results demonstrate that electron irradiation stimulates the development of collective processes in amorphous alloy systems. It is interesting to note, however, that electron beams of high energy are not required

for excitation of collective motion in these alloys. Indeed, it is known²⁰ that the average electron energy loss above $W_0 \sim 1$ MeV is due mainly to bremsstrahlung, while that below $W_0 \sim 1$ MeV is due principally to ionization or excitation of the target material. It has been shown³⁹ that a reduced average energy loss ($-dW^*/dx$) can be defined such that a physical quantity independent of the elemental parameters (atomic number Z , atomic weight A , number of atoms per cubic centimeter N) is obtained. The reduced average energy loss ($-dW^*/dx$) is the average energy loss ($-dW/dx$) (expressed in MeV/cm of target material) divided by the product $ZN\phi_0$, where $\phi_0 = 8\pi R_0^2/3 = 6.653 \times 10^{-25}$ cm², with R_0

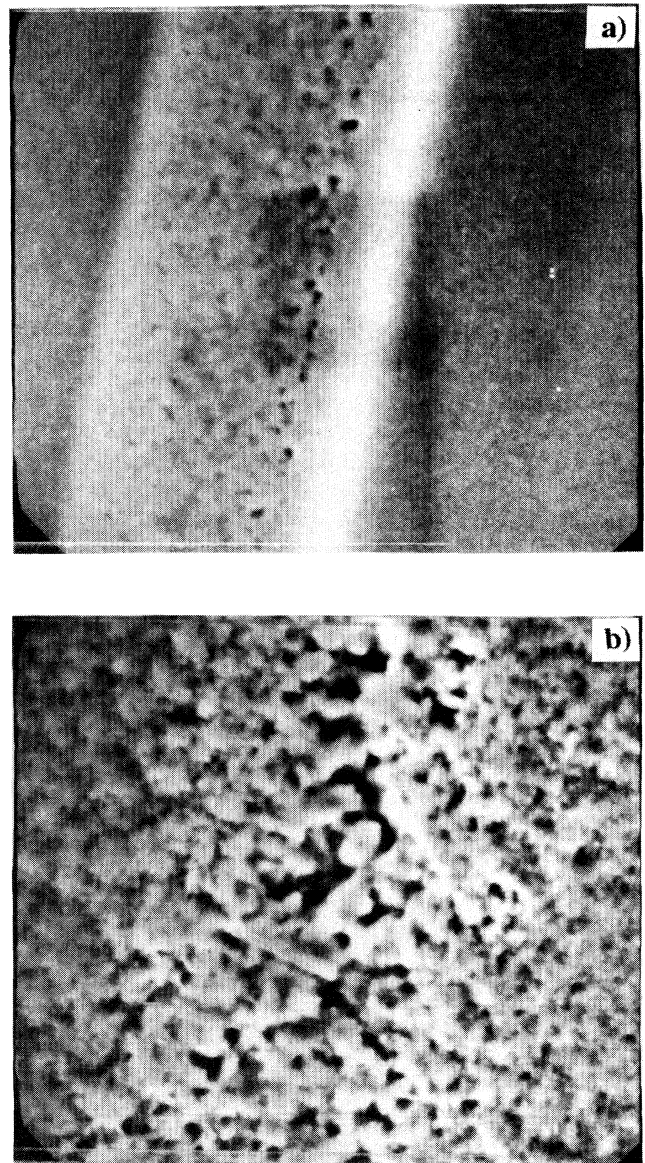


FIG. 4. SEM examinations of the $\text{Fe}_{81}\text{B}_{13.5}\text{Si}_{3.5}\text{C}_2$ sample, after irradiation with low-energy electrons ($W = 50$ keV, $\Phi_E = 2.4 \times 10^{15}$ electrons/cm²). The magnification employed had the values: (a) $\times 2400$; (b) $\times 2700$.

the classical electron radius $R_0 = 2.818 \times 10^{-13}$ cm. Consequently, published literature data on the reduced average energy loss²⁰ can be used in the present study to characterize the interaction of electrons with metallic alloy systems. Such estimates show that 7-MeV electrons lose only $\sim 0.1\%$ of their energy while interacting with the 20- μm -thick amorphous alloy foil, whereas the electrons having an energy of 50 and 30 keV transfer $\sim 60\%$ and, respectively, 100% of their energy to the irradiated material. These calculations suggest that high-energy electrons are not likely to significantly change the phase composition of metallic glasses, whereas low-energy electrons can give rise to temperature gradients and enhance the motion of diffusional material. Crystalline regions may subsequently arise in the irradiated alloy system.

C. Pulsed-excimer-laser irradiation effects in amorphous and thermally annealed $\text{Fe}_{81}\text{B}_{13.5}\text{Si}_{3.5}\text{C}_2$ metallic glass

Room-temperature transmission Mössbauer spectra of the $\text{Fe}_{81}\text{B}_{13.5}\text{Si}_{3.5}\text{C}_2$ samples, in the amorphous as-quenched state and after pulsed-excimer-laser irradiation ($\lambda = 308$ nm, $\tau = 10$ ns) with 2, 5, and 10 laser pulses per spot as a laser fluence of 5×10^{18} photons/cm² and a repetition rate of 1 Hz are shown in Figs. 5(a)–5(d). The corresponding hyperfine magnetic field distributions extracted from these spectra are shown in Figs. 5(A)–5(D). The refined values of the hyperfine parameters corresponding to the as-quenched and pulsed-laser-treated $\text{Fe}_{81}\text{B}_{13.5}\text{Si}_{3.5}\text{C}_2$ samples are listed in Table III.

It can be seen in Fig. 5(b), for the $\text{Fe}_{81}\text{B}_{13.5}\text{Si}_{3.5}\text{C}_2$ sam-

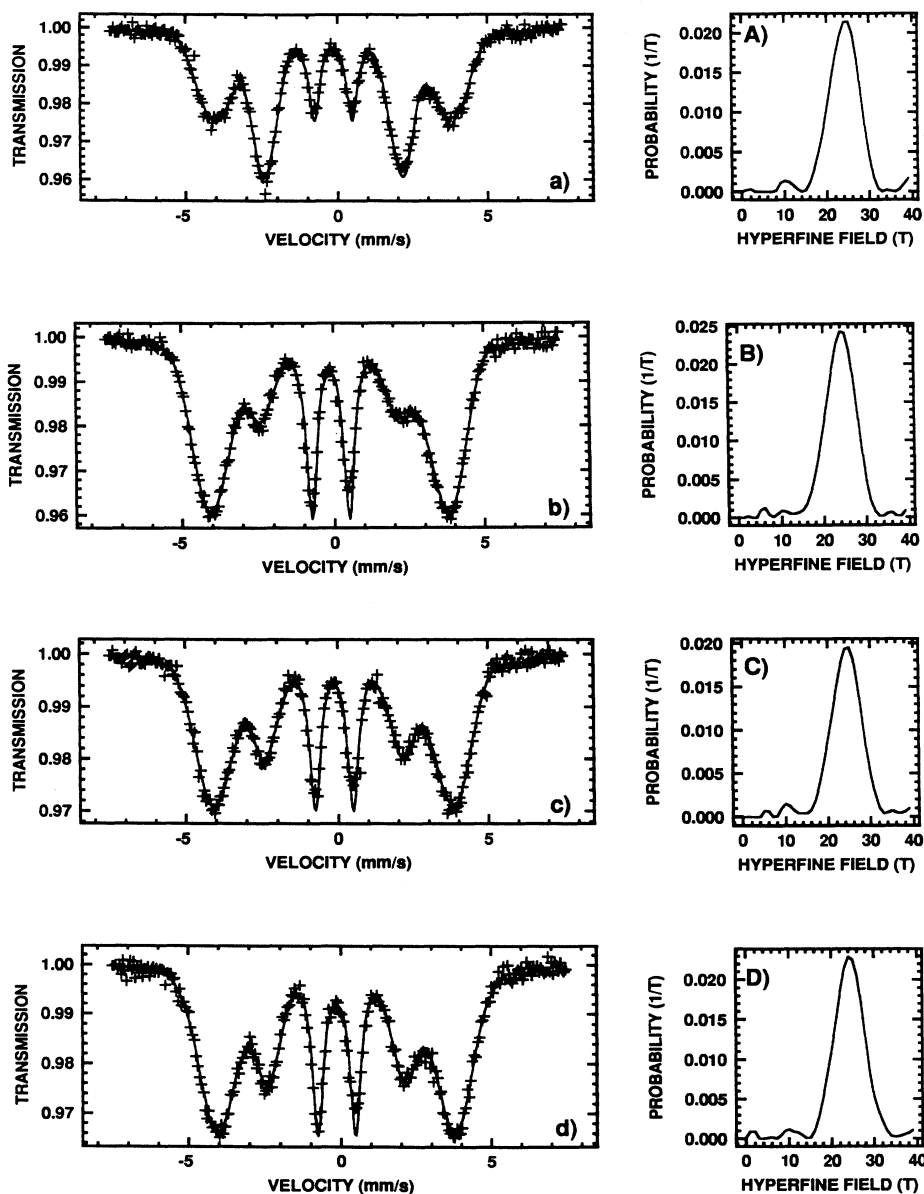


FIG. 5. Room-temperature transmission Mössbauer spectra of the $\text{Fe}_{81}\text{B}_{13.5}\text{Si}_{3.5}\text{C}_2$ samples: (a) in the amorphous as-quenched state and after pulsed-excimer-laser irradiation ($\lambda = 308$ nm, $\tau = 10$ ns, $\Phi_L = 5 \times 10^{18}$ photons/cm², repetition rate 1 Hz) with (b) 2 laser pulses/spot; (c) 5 laser pulses/spot; (d) 10 laser pulses/spot. The corresponding hyperfine magnetic-field distributions are shown in (A)–(D).

TABLE III. Relative intensity of lines R_{21} , average hyperfine magnetic field $\langle H_{\text{hf}} \rangle$, mean hyperfine field $(H_{\text{hf}})_m$, width of the hyperfine magnetic-field distribution ΔH_{hf} , and total absorption area in the Mössbauer spectra of the $\text{Fe}_{81}\text{B}_{13.5}\text{Si}_{3.5}\text{C}_2$ samples, as a function of the number of applied laser pulses N .

N (laser pulses)	R_{21}	$\langle H_{\text{hf}} \rangle$ (kOe)	$(H_{\text{hf}})_m$ (kOe)	ΔH_{hf} (kOe)	Resonant area (a.u.)
0	1.11	251.1	255.2	45.5	0.219
2	0.26	249.5	255.1	45.7	0.220
5	0.41	253.2	257.3	46.5	0.178
10	0.43	251.3	256.9	47.6	0.208
Errors:	± 0.02	± 2.5	± 2.5	± 2.5	± 0.005

ple irradiated with 2 laser pulses per spot, that laser-induced effects have resulted in a pronounced decrease of the intensity ratio of the second to the first line. The corresponding value of the magnetic texture parameter R_{21} (Table III) shows that a rotation of the average magnetic-moment direction from the in-plane to an out-of-plane orientation has taken place. For the $\text{Fe}_{81}\text{B}_{13.5}\text{Si}_{3.5}\text{C}_2$ samples irradiated with 5 and 10 laser pulses per spot [Figs. 5(c) and 5(d), respectively], the areal intensity ratio R_{21} progressively increases as compared to the spectrum in Fig. 5(b), but remains different from the value indicating the random distribution of magnetic-moment directions. Consequently, the average direction of bulk magnetization in $\text{Fe}_{81}\text{B}_{13.5}\text{Si}_{3.5}\text{C}_2$ maintains an out-of-plane orientation upon increasing the number of applied pulses during excimer-laser irradiation. This behavior is in qualitative agreement with the dependence of the intensity ratio R_{21} on the repetition rate, as determined by isochronal excimer-laser annealing of iron-based and nickel-iron-based alloy samples.⁹ As can be seen in Table III, however, the average hyperfine magnetic field $\langle H_{\text{hf}} \rangle$, width of the field distribution ΔH_{hf} , and total absorption area in the Mössbauer spectra show no significant variations during the laser treatment performed, suggesting the absence of crystallization effects in the irradiated $\text{Fe}_{81}\text{B}_{13.5}\text{Si}_{3.5}\text{C}_2$ samples. It can be assumed that the laser-induced magnetic anisotropy observed in the present study is related to the formation of stresses in the $\text{Fe}_{81}\text{B}_{13.5}\text{Si}_{3.5}\text{C}_2$ amorphous system, due to the high heating and cooling rates associated with nanosecond pulsed-laser irradiation. Indeed, it has been shown⁴⁰ that in magnetic specimens, due to magnetoelastic effects, internal stresses generated by surface modifications may dramatically change the bulk magnetic properties. Consequently, we find that the average magnetization direction in $\text{Fe}_{81}\text{B}_{13.5}\text{Si}_{3.5}\text{C}_2$ can be controlled by the number of applied laser pulses without inducing crystallization. These findings suggest that laser processing of iron-based metallic glasses promotes control over important material characteristics which has not been achieved using conventional processing methods.

Recent investigations⁹ have demonstrated the effect of excimer-laser-induced crystallization in an $\text{Fe}_{77}\text{Cr}_2\text{B}_{16}\text{Si}_5$ amorphous alloy by employing high repetition rates and

laser fluences. In order to gain additional information on the fundamental effects underlying the interaction of laser radiation with metallic glasses, the present study investigates the influence of pulsed-excimer-laser treatment on the phase composition of thermally annealed $\text{Fe}_{81}\text{B}_{13.5}\text{Si}_{3.5}\text{C}_2$ samples.

Figure 6(a) shows the room-temperature transmission Mössbauer spectrum of the $\text{Fe}_{81}\text{B}_{13.5}\text{Si}_{3.5}\text{C}_2$ sample, after thermal annealing at 375 °C for 1 h. The corresponding hyperfine magnetic-field distribution is given in Fig. 6(A), while the fitted values of the hyperfine parameters are listed in Table IV. Although the bulk Mössbauer results are indicative of amorphous phase, the slight decrease in the relative intensity R_{21} as compared to the as-quenched state (Table III) suggests the formation of partially crystallized surface layers. Indeed, it has been shown²¹ that the generation of crystalline precipitates of higher density with respect to the amorphous phase causes compressive stresses in the bulk of the specimens with positive magnetostriction, which tend to rotate the atomic spins in a direction out of the ribbon plane. This thermally annealed sample was further exposed to pulsed-excimer-laser irradiation ($\lambda=308$ nm, $\tau=10$ ns) with 2 laser pulses per spot at a repetition rate of 1 Hz, using a single-pulse laser fluence of 5×10^{18} photons/cm². The room-temperature transmission Mössbauer spectrum and hyperfine magnetic-field distribution of the irradiated $\text{Fe}_{81}\text{B}_{13.5}\text{Si}_{3.5}\text{C}_2$ sample are shown in Figs. 6(b) and 6(B), respectively. It can be inferred from Table IV that a pronounced out-of-plane reorientation of the bulk magnetization direction has resulted as a consequence of the laser treatment performed. As in the case of the $\text{Fe}_{81}\text{B}_{13.5}\text{Si}_{3.5}\text{C}_2$ sample subjected to irradiation in the as-quenched state, the development of laser-induced magnetic anisotropy in the thermally annealed $\text{Fe}_{81}\text{B}_{13.5}\text{Si}_{3.5}\text{C}_2$ specimen is not accompanied by the onset of bulk crystallization. However, distinctive features regarding the laser-induced surface modifications can be observed in the SEM examinations of the $\text{Fe}_{81}\text{B}_{13.5}\text{Si}_{3.5}\text{C}_2$ sample, performed after thermal annealing and subsequent laser irradiation [Fig. 7(a)]. SEM investigations (top of the micrograph) demonstrate the presence of crys-

TABLE IV. Relative intensity of lines R_{21} , average hyperfine magnetic field $\langle H_{\text{hf}} \rangle$, mean hyperfine field $(H_{\text{hf}})_m$, and width of the hyperfine magnetic-field distribution ΔH_{hf} of the amorphous component in the as-annealed and laser-irradiated $\text{Fe}_{81}\text{B}_{13.5}\text{Si}_{3.5}\text{C}_2$ samples.

Treatment of samples	R_{21}	$\langle H_{\text{hf}} \rangle$ (kOe)	$(H_{\text{hf}})_m$ (kOe)	ΔH_{hf} (kOe)
375 °C, 1 h, as-annealed	0.82	249.6	254.6	45.9
375 °C, 1 h, laser-irradiated	0.33	248.2	253.9	48.2
450 °C, 1 h, as-annealed ^a	0.67	250.5	254.7	49.5
450 °C, 1 h, laser-irradiated	0.37	248.6	254.4	50.2
Errors:	± 0.02	± 1.2	± 1.2	± 1.5

^aThe sample also contains 11.9% α -Fe ($H_{\text{hf}}=330.8$ kOe, $R_{21}=0.88$).

talline precipitates on the surface of the thermally annealed $\text{Fe}_{81}\text{B}_{13.5}\text{Si}_{3.5}\text{C}_2$ sample prior to the laser treatment performed. Their existence was previously assumed in order to explain the change in the direction of the net magnetic moment in the heat-treated $\text{Fe}_{81}\text{B}_{13.5}\text{Si}_{3.5}\text{C}_2$ sample. The nature of these surface precipitates was identified by EDX analysis of the corresponding microvolumes [Fig. 7(b)], which revealed the segregation of crystalline iron in the near-surface region. The most interesting feature in Fig. 7(a), however, is represented by the region of the laser pulse incidence on the surface of the thermally annealed $\text{Fe}_{81}\text{B}_{13.5}\text{Si}_{3.5}\text{C}_2$ sample (bottom of the micrograph). The uniform aspect of the laser-irradiated area is indicative of amorphous phase formation, due to laser-induced melting and rapid solidification. This demonstrates that the laser treatment performed resulted in the redissolution of the precipitate particles. The mol-

ten zones which subsequently resolidified following pulsed-laser irradiation give rise to complex internal stresses, which are responsible for the observed out-of-plane reorientation of the easy magnetization axis.

In order to further investigate the effect of excimer-laser-induced amorphization, a partially crystallized $\text{Fe}_{81}\text{B}_{13.5}\text{Si}_{3.5}\text{C}_2$ sample was prepared by annealing the as-quenched specimen at 450°C for 1 h. The room-temperature transmission Mössbauer spectrum and hyperfine magnetic-field distribution of the thermally annealed $\text{Fe}_{81}\text{B}_{13.5}\text{Si}_{3.5}\text{C}_2$ sample are shown in Figs. 6(c) and 6(C), respectively. The six-line pattern in the Mössbauer spectrum corresponds to the α -Fe crystalline phase, which represents 11.9% of the sample composition. The hyperfine magnetic-field distribution is associated with the remaining amorphous matrix, in which the random distribution of magnetic-moment directions has resulted

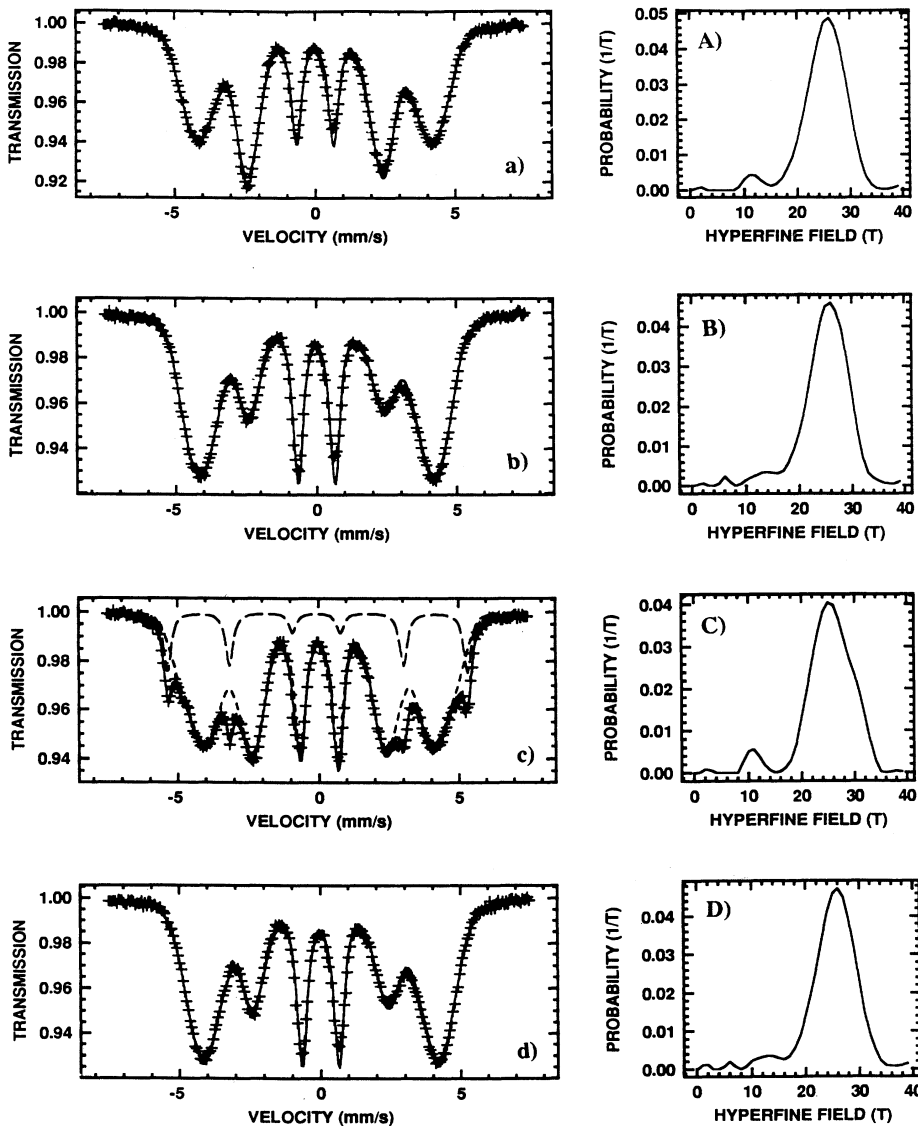


FIG. 6. Room-temperature transmission Mössbauer spectra of the $\text{Fe}_{81}\text{B}_{13.5}\text{Si}_{3.5}\text{C}_2$ samples, after thermal annealing and subsequent pulsed-excimer-laser irradiation: (a) sample annealed at 375°C for 1 h, (b) sample annealed at 375°C for 1 h and excimer-laser irradiated; (c) sample annealed at 450°C for 1 h; (d) sample annealed at 450°C for 1 h and excimer-laser irradiated. The treatment was carried out at a laser fluence $\Phi_L = 5 \times 10^{18}$ photons/cm². The corresponding hyperfine magnetic-field distributions extracted from the Mössbauer spectra are presented in (A)–(D).

(Table IV). The partially crystallized sample was further exposed to pulsed-excimer-laser irradiation ($\Phi_L = 5 \times 10^{18}$ photons/cm²) with 2 laser pulses per spot at a repetition rate of 1 Hz. The room-temperature transmission Mössbauer spectrum and hyperfine magnetic-field distribution of the irradiated Fe₈₁B_{13.5}Si_{3.5}C₂ sample are shown in Figs. 6(d) and 6(D), respectively. The bulk Mössbauer measurements show that the composition of the irradiated specimen is entirely amorphous, with a pronounced out-of-plane reorientation of the magnetic-moment directions (as indicated by the corresponding R_{21} value in Table IV). Consequently, the effect of excimer-laser-induced amorphization was evidenced in the partially crystallized Fe₈₁B_{13.5}Si_{3.5}C₂ system and was found to be accompanied by the development of laser-induced magnetic anisotropy. The re vitrification process originates in the molten zones subsequently quenched due to pulsed-excimer-laser irradiation, while the mechanical stresses

associated with rapid heating and cooling are suggested to be responsible for the reorientation of the easy magnetization axis. A typical region formed as an effect of excimer-laser-induced amorphization is shown in the SEM photograph of Fig. 8(a). The laser-irradiated zone in which the phase transformation has taken place corresponds to the top of the micrograph, whereas the surface morphology of the partially crystallized Fe₈₁B_{13.5}Si_{3.5}C₂ sample prior to laser irradiation can be examined at the bottom of the SEM micrograph. This region exhibits α -Fe crystalline precipitates with typical dimensions in the range 50–90 nm, although some micron-size crystallites are also observed [Fig. 8(b)].

In order to explain the effect of excimer-laser-induced amorphization in the metallic glass studied and obtain

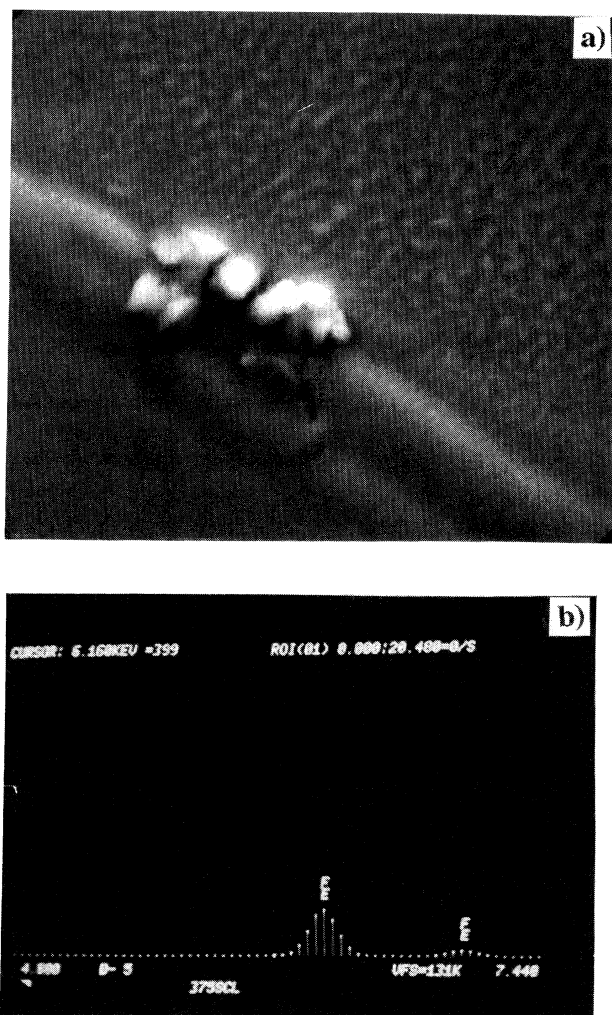


FIG. 7. (a) SEM photograph ($\times 2000$) and (b) EDX examination of the Fe₈₁B_{13.5}Si_{3.5}C₂ sample, after thermal annealing at 375°C for 1 h, followed by pulsed-excimer-laser treatment ($\lambda = 308$ nm, $\tau = 10$ ns, $\Phi_L = 5 \times 10^{18}$ photons/cm²).

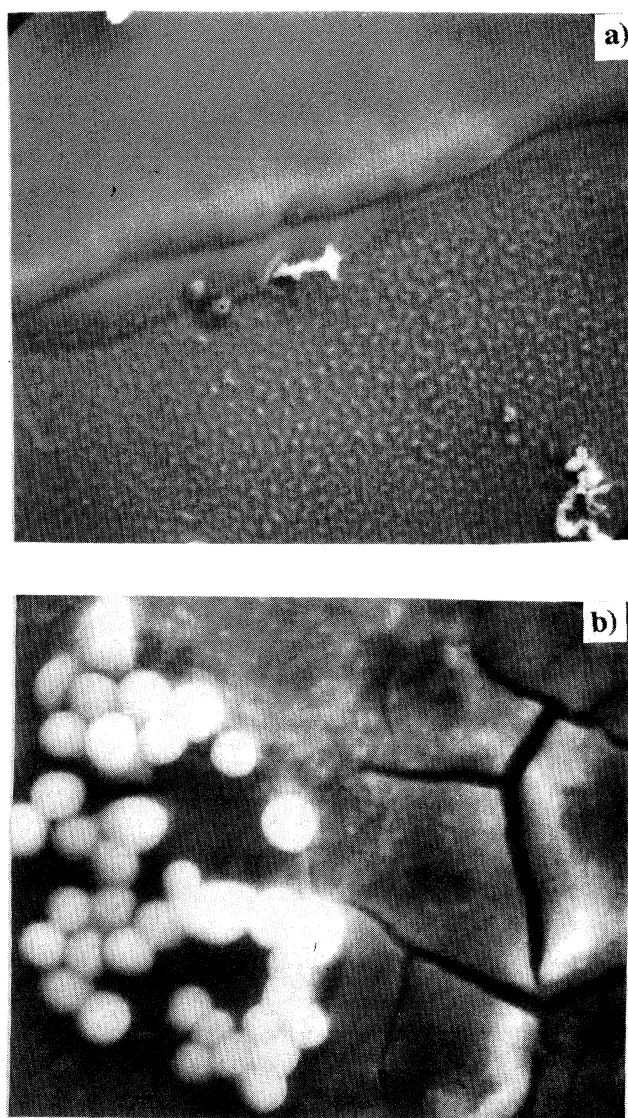


FIG. 8. SEM examinations of the Fe₈₁B_{13.5}Si_{3.5}C₂ sample, after thermal annealing at 450°C for 1 h and subsequent pulsed-excimer-laser irradiation ($\lambda = 308$ nm, $\tau = 10$ ns, $\Phi_L = 5 \times 10^{18}$ photons/cm²). The magnification employed had the values: (a) $\times 1000$; (b) $\times 3000$.

order-of-magnitude predictions regarding the kinetics of laser-induced phase transformation, melt model calculations must be considered. Thus, the depth of the molten layer (d) formed during an intense laser pulse of duration τ is $d = (2D\tau)^{1/2}$, where D is the heat diffusivity of the material. Considering the D value for $\text{Fe}_{81}\text{B}_{13.5}\text{Si}_{3.5}\text{C}_2$ of $^{41} D \sim 3 \text{ mm}^2/\text{s}$, d is found to be $\sim 240 \text{ nm}$ for 10-ns laser pulses. Considering the experimental data available for silicon,⁴² a lifetime of the molten layer (t_m) of 400 ns is expected. Assuming a similar behavior of metals and a diffusivity in the liquid phase $D_l \sim 10^{-4} \text{ cm}^2/\text{s}$, the mixing length $\Lambda = (D_l t_m)^{1/2} \sim 70 \text{ nm}$ is found to be comparable with the dimensions of the surface crystalline precipitates. Since the mixing length defines an upper limit for the influence of nanosecond laser irradiation of the surface inhomogeneities, one can infer from the above calculations that pulsed-excimer-laser irradiation is an effective method for restoring the amorphous structure of metallic glass specimens.

IV. CONCLUSIONS

Radiation can have both the effect of ordering a disordered system and of disordering an ordered system. Instances of both effects have been revealed in the present study. The main results can be summarized as follows:

(i) High-energy electron-beam irradiation of the amor-

phous $\text{Fe}_{81}\text{B}_{13.5}\text{Si}_{3.5}\text{C}_2$ system was found to induce an out-of-plane magnetic anisotropy due to changes in the chemical short-range order.

(ii) Low-energy electron-beam irradiation of $\text{Fe}_{81}\text{B}_{13.5}\text{Si}_{3.5}\text{C}_2$ resulted in the formation of stable regions with different crystalline structures, in which α -Fe, Fe-Si, Fe_3B , and Fe_2B crystalline phases, as well as γ -Fe clusters could be identified. Low-energy electron irradiation was shown to stimulate the development of collective processes in the amorphous alloy system, which were interpreted in terms of radiation-enhanced diffusion.

(iii) In addition to inducing controlled magnetic anisotropy in the amorphous $\text{Fe}_{81}\text{B}_{13.5}\text{Si}_{3.5}\text{C}_2$ system, pulsed-excimer-laser irradiation was shown to cause revitrification of partially crystallized $\text{Fe}_{81}\text{B}_{13.5}\text{Si}_{3.5}\text{C}_2$ samples. The effect of pulsed-excimer-laser-induced amorphization was evidenced and explained using melt model calculations.

(iv) Microstructure development, as inferred from Mössbauer spectrometry and complementary techniques is fraught with information regarding the radiation-driven property modifications in amorphous systems.

ACKNOWLEDGMENTS

This work has been supported by the National Science Foundation and the Office of Naval Research.

- ¹M. Miglierini and I. Skorvanek, *Mater. Sci. Eng. A* **147**, 101 (1991).
- ²M. Miglierini and J. Sitek, *Key Eng. Mater.* **40-41**, 281 (1990).
- ³G. Serfözö, L. F. Kiss, C. S. Daroczi, E. Kisdi-Koszo, G. Vertesy, and A. Slawska-Waniewska, *IEEE Trans. Magn.* **26**, 1418 (1990).
- ⁴L. Lanotte, C. Luponio, and F. Porreca, *J. Magn. Magn. Mater.* **61**, 225 (1986).
- ⁵L. Lanotte, P. Matteazzi, and V. Tagliaferri, *J. Magn. Magn. Mater.* **42**, 183 (1984).
- ⁶C. Aroca, M. C. Sanchez, I. Tanarro, P. Sanchez, E. Lopez, and M. Vazquez, *Phys. Rev. B* **42**, 8086 (1990).
- ⁷I. T. Collier, M. R. J. Gibbs, and N. Seddon, *J. Magn. Magn. Mater.* **111**, 260 (1992).
- ⁸A. P. Radlinski, A. Calka, and B. Luther-Davies, *Mater. Sci. Eng.* **97**, 253 (1988).
- ⁹M. Sorescu and E. T. Knobbe, *Phys. Rev. B* **49**, 3253 (1994).
- ¹⁰M. Sorescu and E. T. Knobbe, *J. Mater. Res.* **8**, 3078 (1993).
- ¹¹D. Sorescu, M. Sorescu, I. N. Mihailescu, D. Barb, and A. Hening, *Solid State Commun.* **85**, 717 (1993).
- ¹²D. Sorescu, M. Sorescu, A. Hening, I. N. Mihailescu, and D. Barb, *Rom. Rep. Phys.* **44**, 787 (1992).
- ¹³M. Sorescu, E. T. Knobbe, D. Barb, D. Sorescu, and I. Bibicu, *Hyperfine Interact.* **92**, 1347 (1994).
- ¹⁴M. Sorescu, E. T. Knobbe, and D. Barb, *J. Phys. Chem. Solids* (to be published).
- ¹⁵A. Chamberod, J. Laugier, and J. M. Penisson, *J. Magn. Magn. Mater.* **10**, 139 (1979).
- ¹⁶*Metglas Technical Bulletin* (Allied-Signal, Inc., Parsippany, 1994).
- ¹⁷R. A. Brand, J. Lauer, and D. M. Herlach, *J. Phys. F* **13**, 675 (1983).
- ¹⁸J. B. Wachtman, *Characterization of Materials* (Butterworth-Heinemann and Manning, Stoneham, CT, 1993), Chap. 34.
- ¹⁹T. E. Cranshaw and G. Longworth, in *Mössbauer Spectroscopy Applied to Inorganic Chemistry*, edited by G. J. Long (Plenum, New York, 1984), Vol. 1, p. 173.
- ²⁰J. W. Corbett, in *Electron Radiation Damage in Semiconductors and Metals*, edited by F. Seitz and D. Turnbull (Academic, New York, 1966), Vol. 7, p. 35.
- ²¹H. N. Ok and A. H. Morrish, *Phys. Rev. B* **23**, 2257 (1981).
- ²²N. Saegusa and A. H. Morrish, *Phys. Rev. B* **26**, 305 (1982).
- ²³M. S. Rogalski, I. Bibicu, and M. Sorescu, *Hyperfine Interact.* **92**, 1317 (1994).
- ²⁴I. Nowik, I. Felner, Y. Wolfus, and Y. Yeshurun, *J. Phys. F* **18**, 119 (1988).
- ²⁵T. Egami, *J. Mater. Sci.* **13**, 2587 (1978).
- ²⁶M. Miglierini, *J. Phys. Condens. Matter* **6**, 1431 (1994).
- ²⁷D. Barb, I. Bibicu, M. S. Rogalski, and M. Sorescu, *Hyperfine Interact.* **94**, 2187 (1994).
- ²⁸M. Sorescu, S. Stenger, and U. Gonser, *Phys. Status Solidi A* **132**, K57 (1992).
- ²⁹J. C. Swartz, R. Kossowski, J. J. Haugh, and R. F. Krause, *J. Appl. Phys.* **50**, 7609 (1979).
- ³⁰K. Fukamichi, M. Kikuchi, S. Arakawa, and T. Masumoto, *Solid State Commun.* **23**, 955 (1977).
- ³¹T. Kemeny, I. Vincze, and B. Fogarassy, *Phys. Rev. B* **20**, 476 (1979).
- ³²S. Stenger, M. Sorescu, and U. Gonser, *J. Non-Cryst. Solids* **151**, 66 (1992).
- ³³R. D. Greenough and M. Schultze, *Nondestr. Test. Eval.* **5**, 263 (1990).
- ³⁴O. T. Inal, L. E. Murr, and F. G. Yost, *Mater. Sci. Eng.* **51**, 101 (1981).

- ³⁵W. Keune, T. Ezawa, W. A. A. Macedo, U. Glos, K. P. Schletz, and U. Kirschbaum, *Physica B* **161**, 269 (1989).
- ³⁶M. Acet, H. Zähres, E. F. Wassermann, and W. Pepperhoff, *Phys. Rev. B* **49**, 6012 (1994).
- ³⁷I. A. Dubovtsev, V. N. Grazhdankin, G. M. Vereshkov, and N. F. Losev, *Izv. Akad. Nauk SSSR Ser. Fiz.* **52**, 1711 (1988) [*Bull. Acad. Sci. USSR Phys. Ser.* **52**, 45 (1988)].
- ³⁸J. W. Corbett, in *Electron Radiation Damage in Semiconductors and Metals* (Ref. 20), p. 294.
- ³⁹W. Heitler, *Quantum Theory of Radiation* (Oxford University Press, London, 1954), Chap. 37.
- ⁴⁰G. Herzer and H. R. Hilzinger, *J. Magn. Magn. Mater.* **62**, 143 (1986).
- ⁴¹L. Lanotte, A. Annunziata, P. Silvestrini, and V. Tagliaferri, *Nuovo Cimento* **13D**, 1123 (1991).
- ⁴²G. E. Jellison, Jr., D. H. Lowndes, and R. F. Wood, in *Excimer Lasers and Optics*, edited by T. S. Luk, Proc. SPIE Vol. 710 (SPIE, Bellingham, WA, 1986), p. 24.

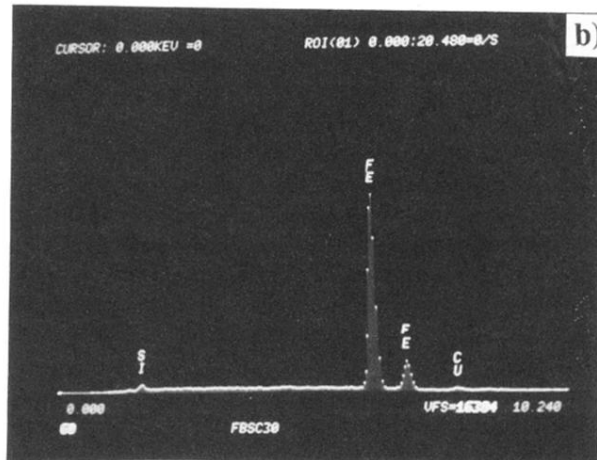
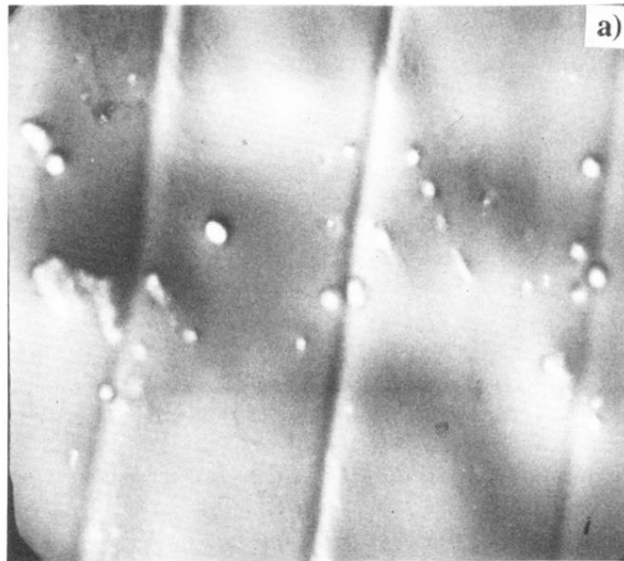


FIG. 2. (a) SEM photograph ($\times 1500$) and (b) EDX examination of the $\text{Fe}_{81}\text{B}_{13.5}\text{Si}_{3.5}\text{C}_2$ sample, after low-energy electron-beam irradiation ($W = 30$ keV, $\Phi_E = 2.4 \times 10^{15}$ electrons/cm²). Fe and Si peaks stand for the sample, whereas Cu impurities come from the tape.

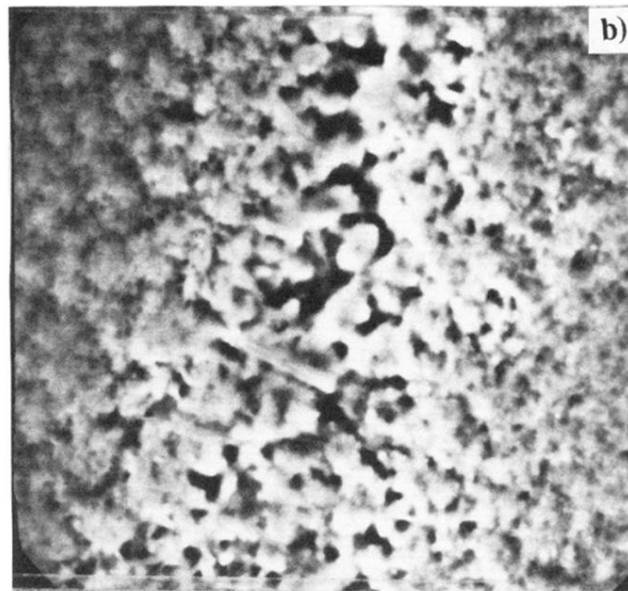
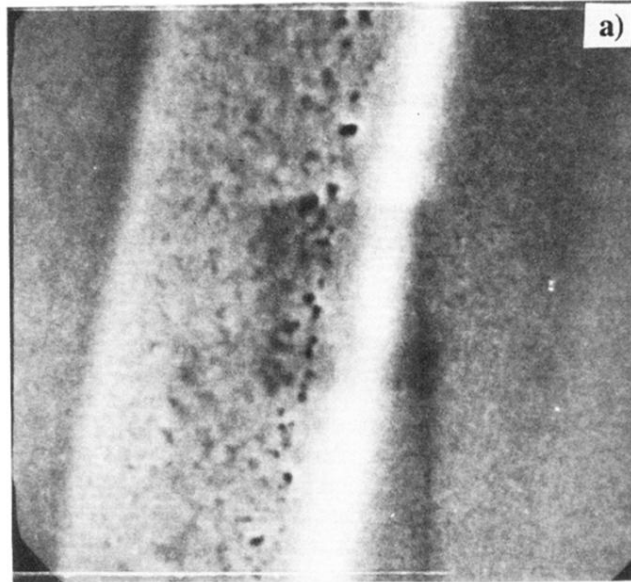


FIG. 4. SEM examinations of the $\text{Fe}_{81}\text{B}_{13.5}\text{Si}_{3.5}\text{C}_2$ sample, after irradiation with low-energy electrons ($W=50$ keV, $\Phi_E=2.4\times 10^{15}$ electrons/cm²). The magnification employed had the values: (a) $\times 2400$; (b) $\times 2700$.

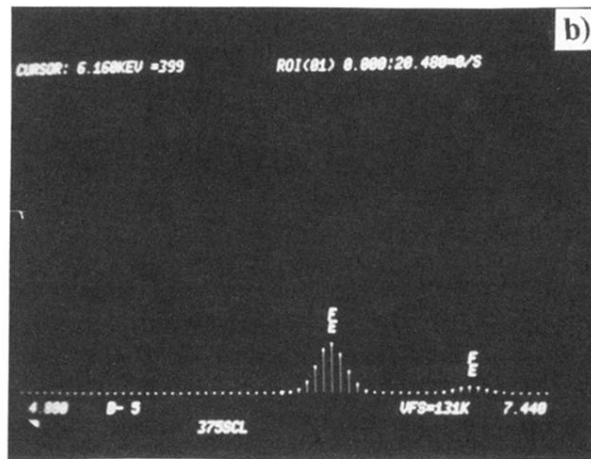
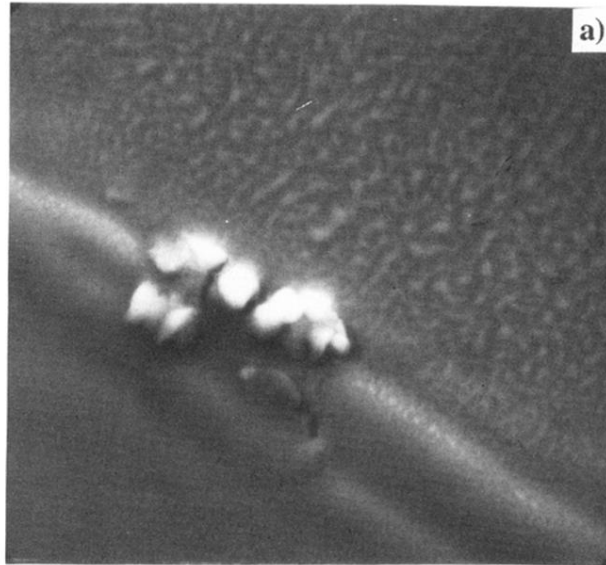


FIG. 7. (a) SEM photograph ($\times 2000$) and (b) EDX examination of the $\text{Fe}_{81}\text{B}_{13.5}\text{Si}_{3.5}\text{C}_2$ sample, after thermal annealing at 375°C for 1 h, followed by pulsed-excimer-laser treatment ($\lambda = 308 \text{ nm}$, $\tau = 10 \text{ ns}$, $\Phi_L = 5 \times 10^{18} \text{ photons/cm}^2$).

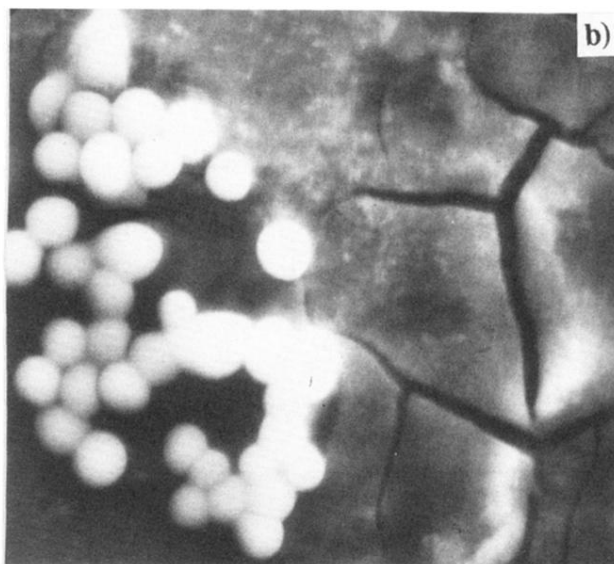


FIG. 8. SEM examinations of the $\text{Fe}_{81}\text{B}_{13.5}\text{Si}_{3.5}\text{C}_2$ sample, after thermal annealing at 450°C for 1 h and subsequent pulsed-excimer-laser irradiation ($\lambda=308$ nm, $\tau=10$ ns, $\Phi_L=5\times 10^{18}$ photons/ cm^2). The magnification employed had the values: (a) $\times 1000$; (b) $\times 3000$.